Steel and Composite Structures, *Vol. 33, No. 4* (*2019*) *615-627*
DOI: https://doi.org/10.12989/scs.2019.33.4.615

Compressive behavior of circular hollow and concrete-filled steel tubular stub columns under atmospheric corrosion

Shan Gao[*1,2], Zhen Peng [1a], Xuanding Wang [2b] and Jiepeng Liu [3c]

[1] *Shaanxi Key Laboratory of safety and durability of concrete structures*, *Xijing University*, *Xi'an*, *China*
[2] *Postdoctoral Station of Civil Engineering*, *Chongqing University*, *Chongqing*, *China*
[3] *School of Civil Engineering*, *Chongqing University*, *Chongqing*, *China*

(*Received July 19, 2019, Revised September 30, 2019, Accepted October 7, 2019*)

Abstract. This paper aims to study the compressive behavior of circular hollow and concrete-filled steel tubular stub columns under simulated marine atmospheric corrosion. The specimens after salt spray corrosion were tested under axial compressive load. Steel grade and corrosion level were mainly considered in the study. The mechanical behavior of circular CFST specimens is compared with that of the corresponding hollow ones. Design methods for circular hollow and concrete-filled steel tubular stub columns are modified to consider the effect of marine atmospheric corrosion. The results show that linear fitting curves could be used to present the relationship between corrosion rate and the mechanical properties of steel after simulated marine atmospheric corrosion. The ultimate strength of hollow steel tubular and CFST columns decrease with the increase of corrosion rate while the ultimate displacement of those are hardly affected by corrosion rate. Increasing corrosion rate would change the failure of CFST stub column from ductile failure to brittle failure. Corrosion rate would decrease the ductility indexes of CFST columns, rather than those of hollow steel tubular columns. The confinement factor ξ of CFST columns decreases with the increase of corrosion rate while the ratio between test value and nominal value shows an opposite trend. With considering marine atmospheric corrosion, the predicted axial strength of hollow steel tubular and CFST columns by Chinese standard agree well with the tested values while the predictions by Japanese standard seem conservative.

Keywords: CFST; hollow steel tube; compressive behavior; stub column; simulated marine atmosphere; salt spray corrosion

1. Introduction

Offshore steel structures including bridges, telecommunication towers and civil buildings are exposed to highly corrosive marine environment during their long service lives. Severe surface corrosion of steel offshore structures would result in many harmful consequences including strength degradation, thickness penetration, fatigue cracks and brittle failure (Wang *et al*. 2017a), especially for thin-walled steel structures. Pipe truss and other hollow steel tubular structures are vulnerable to local buckling which would be aggravated by surface corrosion.

Concrete-filled steel tube (CFST) has been widely used in different types of infrastructure in the world, due to its excellent structural performance, economic and constructional benefits (Han *et al*. 2012). Besides these advantages, core concrete would support outer steel tube and prevent it buckling inwardly. To a certain extent, the corroded outer steel tube could be protected by core concrete from inside.

∗Corresponding author, Associate Professor,
E-mail: gaoshan@xijing.edu.cn
[a] Master Student, E-mail: 707892760@qq.com
[b] Ph.D., E-mail: wangxuanding@163.com
[c] Professor, E-mail: liujp@cqu.edu.cn

Depending on the exposure environment, marine corrosion involves four types: immersion, splash/tidal zone, atmospheric and semi-enclosed space (Qin and Cui 2003). Immersion and atmospheric corrosion are the most commonly used methods to simulate marine corrosion in experimental study. It is worth to notice that the composition and form of steel corrosion products in marine atmosphere may differ from those in marine immersion due to different chloride ion and oxygen content (Wang *et al*. 2015).

The mechanism of corrosion on steel and the performance of steel structures including ship structures under marine corrosion have been studied for years. Khedmati *et al.* (2011) proposed an effective method for the strength evaluation of steel plate randomly corroded on both sides under uniaxial compression. Chaves and Melchers (2011) studied pitting corrosion in pipeline steel weld zones. The results revealed that maximum pit depths and pit depth variability both became greater in the heat affected zone. Kaita *et al.* (2012) developed an enhanced method of predicting effective thickness of corroded steel plates. Jiang and Soares (2012) proposed an empirical formula based on FEM results to predict the ultimate strength of pitted plates under in-plane compression. Saad-Eldeen *et al.* (2013) analyzed the ultimate strength of aging ship structures based on tests and simulations. A new stress-strain relationship was developed, considering the residual stresses and the

Copyright © 2019 Techno-Press, Ltd.

ISSN: 1229-9367 (Print), 1598-6233 (Online)

corrosion effect. Wang *et al.* (2017a) proposed the formulas for predicting tensile strength of steel which failed to predict the deformability of steel. Wang and Melchers (2017) conducted an experimental analysis of pitting morphology and pitting depth. The results had implications for the corrosion management in industrial practice. Beaulier *et al.* (2010) provided some recommendations from tests to provide guidance to engineers on how to evaluate compressive capacity of corroded members. Karagah *et al.* (2015) conducted an experimental investigation of short steel columns with localized corrosion. The experimental results were compared with the axial capacities predicted by several design provisions. Zheng *et al.* (2015) conducted an experimental study on seismic behavior of multi-aged steel frame columns in acidic atmospheric environment which provided support for establishing a seismic damage model. Gao *et al.* (2016, 2017) investigated the strength degradation of RC columns wrapped with locally and uniformly corroded steel plates. The results provided a useful reference for the maintenance and strengthening of the in-service columns.

To investigate the performance of CFST members under marine immersion, the research group in Tsinghua University of China (Han 2012, 2014, Hou *et al*. 2016, Hua *et al*. 2019) conducted a series of test and simulation on the performance of circular and square CFST members under sustained load and immersed chloride corrosion. The experimental results improved the traditional design methods for the consideration of combined sustained load and corrosion which were calibrated and evaluated against the test results. Yuan *et al.* (2018, 2019) conducted experimental studies on circular and square CFST columns under cyclic load and acid rain attack. The results showed that the losses of both thickness and yield strength of an outer steel tube caused by corrosion should be taken into account when predicting the ultimate strength of corroded CFST columns. Chen *et al.* (2018) discussed the impacts of corrosion level and axial ratio on the seismic performance of the CFST columns and compared the bending bearing capacity of the specimens under low cyclic load calculated by the relevant specifications.

The literature review has shown that the studies on CFST members under simulated marine corrosion are still limited. More tests should be conducted to provide further experimental evidence that can be used to validate the various numerical and theoretical studies reported for corroded CFST members. In particular, up to date, atmospheric corrosion has not been used in experimental study on the mechanical performance of CFST members under simulated marine corrosion.

This paper aims to study the compressive behavior of circular hollow and concrete-filled steel tubular stub columns in simulated marine atmospheric corrosion. The specimens after salt spray corrosion are tested under axial compressive load. Steel grades and corrosion levels are considered in the test. The corrosion effect on steel material properties is discussed. The mechanical behavior of circular CFST specimen is compared with that of the corresponding hollow steel column. Current design methods for circular hollow and concrete-filled steel tubular stub column are modified to consider the effect of marine atmospheric corrosion.

2. Experimental program

2.1 Preparation of test specimens

Total 32 specimens were fabricated and tested, consisting of 16 hollow steel tubular stub columns and 16

Table 1 Parameters of specimens

No.	Steel/Concrete grade	$L \times D \times t$ /mm	ρ/%	$D_{w,d}$/%
H235-0-1/ H235-0-2	Q235/C30	270 × 90 × 1.78	--	0
H235-5-1/H235-5-2				5
H235-10-1/H235-10-2				10
H235-20-1/H235-20-2				20
H345-0-1/H345-0-2	Q345/C30	270 × 90 × 1.90	--	0
H345-5-1/H345-5-2				5
H345-10-1/H345-10-2				10
H345-20-1/H345-20-2				20
C235-0-1/C235-0-2	Q235/C30	270 × 90 × 1.78	8.4	0
C235-5-1/C235-5-2				5
C235-10-1/C235-10-2				10
C235-20-1/C235-20-2				20
C345-0-1/C345-0-2	Q345/C30	270 × 90 × 1.90	9.0	0
C345-5-1/C345-5-2				5
C345-10-1/C345-10-2				10
C345-20-1/C345-20-2				20

*Note: ρ is steel ratio of section; $D_{w,d}$ is the designed corrosion rate

CFST stub columns. The length-to-diameter ratio was 3 for all specimens to make sure short column behavior. Due to the limitation of test setup, the steel tubes used in the specimens had the same dimension as $L \times D \times t = 270\ mm \times 90\ mm \times 2\ mm$, where L, D and t were the length, external diameter and thickness of the tubes respectively. Normally, the steel ratio of CFST is in the range 4-10% in arch ribs of bridge and 8-10% in building structures (Wang *et al*. 2017b). In that case, 2-mm-thickness tube was chosen for about 10% steel ratio of CFST specimens.

As shown in Table 1, the designation of specimens started with specimen type (H for hollow tube and C for concrete-filled tube), followed by steel grade, corrosion rate, and the number to distinguish specimens with same parameters. Corrosion rate D_w was defined as Eq. (1). The designed corrosion rates $D_{w,d}$ were 5%, 10% and 20% respectively.

$$D_w = (W_0 - W_1)/W_0 \tag{1}$$

where W_0 and W_1 are the weight of specimen before and after the corrosion respectively.

2.2 Material properties

150 × 150 × 150 mm cubes for testing concrete strength and 150 × 150 × 300 mm prisms for testing concrete Young's modulus were cast and cured in the same lab with the specimens. After testing, the average compressive strength and Young's modulus of concrete were 37.2 MPa and 3.03 × 10^4 MPa respectively. The mechanical properties of un-corroded steel coupon are listed in Table 2, where f_y, f_u, E_s and ε_u are the yield strength, ultimate strength, Young's modulus of steel and ultimate strain of steel respectively. Tensile tests on the corroded steel coupons with various corrosion rates were also conducted. The test results would be discussed in section 3.1.

Table 2 Mechanical properties of steel

Steel grade	t/mm	f_y/MPa	f_u/MPa	E_s/10^5MPa	ε_u /%
Q235	1.78	242	474	2.08	35
Q345	1.90	359	531	2.10	30

Table 3 Parameters of salt spray test

	Parameter
NaCl solution	5% (weight percentage)
PH value of initial preparation solution	3.0
PH value of collected solution	3.1
Chamber temperature	50℃±1℃
Saturated air container temperature	63℃±1℃
Duration of salt spray state	4 hours
Duration of dry state	4 hours

2.3 Configuration of salt spray corrosion

Before axial compression test, all specimens were corroded through a salt spray test simulating marine atmospheric corrosion. The concrete was poured to the steel tubes before the salt spray corrosion in which case only the outer surface of steel tube is corroded. According to Chinese standard GB/T 10125 (2012), a standard acetic acid salt spray (AASS) test was conducted. At first, a neutral solution was made by dissolving 5 weight percentage sodium chloride (NaCl) in the water at the temperature of 25°C±2°C. Then moderate amount of acetic acid was added into the neutral solution until the average PH value of the initial preparation solution was in the range of 3.0-3.1 and that of the collected solution was in the range of 3.1-3.3. Compared with neutral salt spray (NSS) test, this acidic solution with acetic acid would accelerate the corrosion of steel producing no new corrosion products. The detailed parameters and the device of salt spray test are shown in Table 3 and Fig. 1 respectively. It should be mentioned that the configuration of salt spray corrosion can hardly represent a real marine atmosphere, since the composition of seawater varies according to the location of the sea. The corrosion method and corrosive solution used in this study could just represent a general situation. The corrosion was supposed to happen at the surface of the steel tube. Therefore, epoxy was used to isolate the top and bottom steel plates of the specimens from the solution.

6 groups of steel coupons (3 groups for Q235 and others for Q345) with the same corrosion rates were corroded in the same chamber with the specimens. Besides testing the tensile strength of corroded steel, these steel coupons were also used to measure the corrosion rate for the column specimens since they corroded in the same condition (Yuan *et al*. 2018). Severe local corrosion was not considered in this test. It was assumed that uniform corrosion which developed from pitting corrosion occurred on the whole

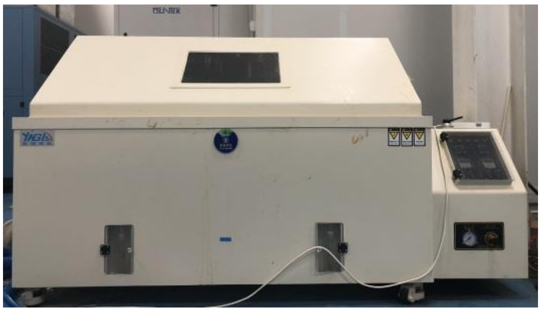

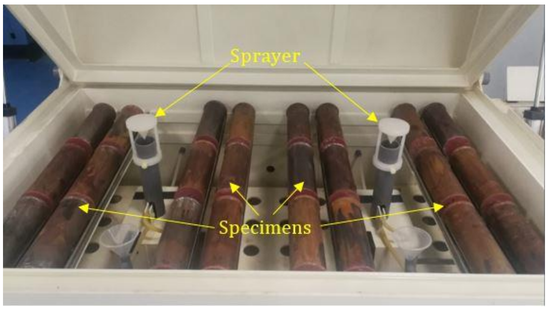

Fig. 1 Salt spray chamber

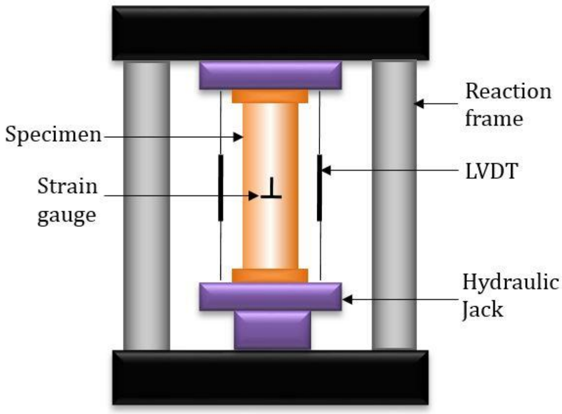

(a) Test setup

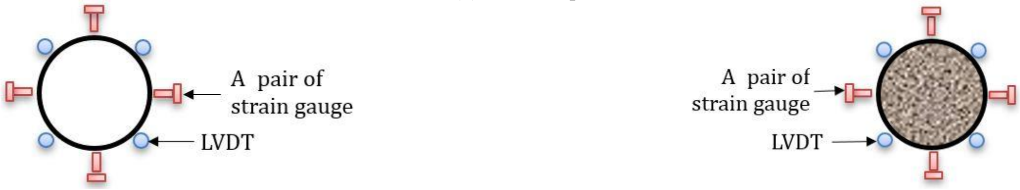

Hollow steel tubular column

CFST column

(b) Measure instruments

Fig. 2 Test setup and measure instruments

$D_w = 0$ $D_w = 5.3\%$

$D_w = 12.5\%$ $D_w = 21.2\%$

Fig. 3 Corroded steel coupons of Q235

surface of specimens.

2.4 Setup of axial compression test

After salt spray test, all the corroded specimens were axially loaded until failure by using a 2000 kN hydraulic compression machine, as shown in Fig. 2(a). Four LVDTs were installed to record the axial deformation of the specimens. Four pairs of strain gauges were evenly spaced around the external surface of concrete-filled steel tubes and hollow steel tubes respectively, as shown in Fig. 2(b).

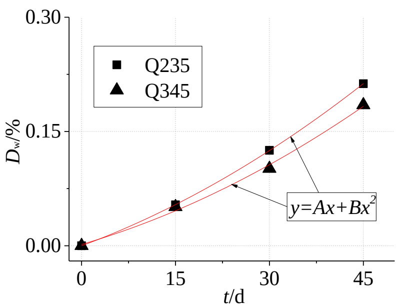

Fig. 4 Relationship of corrosion rate with time

3. Experimental results

3.1 Corrosion effect on steel material properties

The Q235 steel coupons with different corrosion level are shown in Fig. 3. With the increase of corrosion rate, the pitting corrosion spread to the whole surface and tended to uniform corrosion. Fig. 4 shows the relationship between corrosion rate and time. It could be seen that with the increase of corrosion time, the corrosion rate of Q235 steel is exceeding that of Q345 steel. A model proposed by Melchers (2003) for natural marine climate is shown in Fig. 5. As the model depicts, the corroded steel coupons in this study are assumed in the phase 1 and phase 2, since this accelerated salt spray corrosion test was only conducted over 45 days (Melchers 2003). However, the trends of the corroded steel under atmospheric corrosion cannot be present by the mathematical model in Fig. 5, since the curve

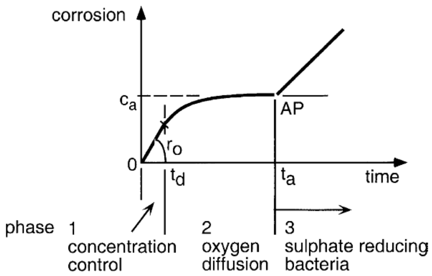

Fig. 5 Mathematical model (Melchers 2003)

in phase 1 and phase 2 of the model is convex while the curve from the test data in this study is concave. In that case, a quadratic equation with two constants is used to describe the relationship of corrosion rate with time. The constant pairs (A, B) for Q235 and Q345 steel are (0.00304, 3.75E-5) and (0.00241, 3.61E-5) respectively.

The mechanical properties of the corroded steel coupons are listed in Table 4. Fig. 6 shows the effects of corrosion

Table 4 Material properties of steel (average value for three coupons in one group)

	f_y/MPa	f_u /MPa	E_s /10^5MPa	ε_u /%	D_w /%
Q235	242	474	2.08	35	0
	222	452	1.97	29	5.3
	200	399	1.85	21	12.5
	174	308	1.69	13	21.2
Q345	359	531	2.10	30	0
	322	518	2.00	25	5.1
	296	488	1.89	19	10.1
	254	423	1.72	11	18.5

rate on mechanical properties of steel. The simulated marine atmospheric corrosion would cause the degradation of tensile properties of steel. Linear fitting curves could be used to present the relationship between corrosion rate and the mechanical properties of corroded steel as follows

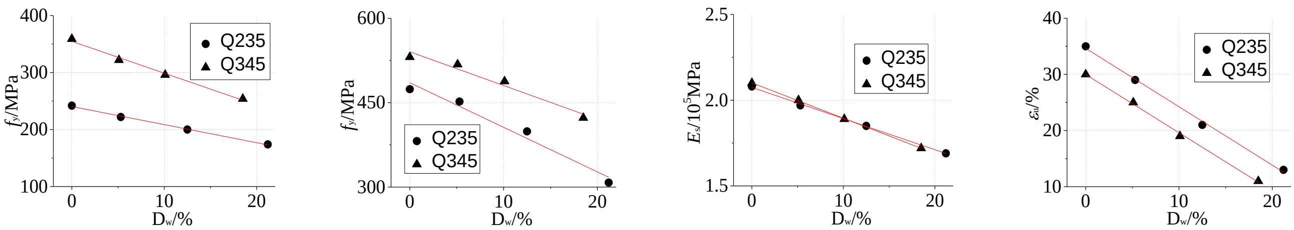

(a) Yield strength (b) Ultimate strength (c) Elastic modulus (d) Ultimate strain

Fig. 6 Effects of corrosion rate on mechanical properties of steel

(a) H235-0 (Type HA) (b) H235-5 (Type HA) (c) H235-10 (Type HA) (d) H235-20 (Type HC)

(e) H345-0 (Type HB) (f) H345-5 (Type HB) (g) H345-10 (Type HC) (h) H345-20 (Type HC)

Fig. 7 Failure modes of hollow steel tubular columns

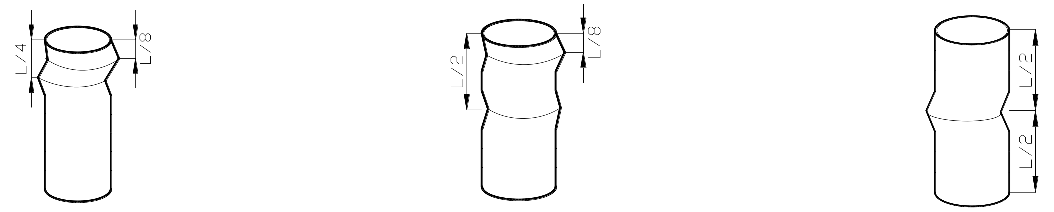

(a) Type HA (Eighth-quarter buckling) (b) Type HB (Eight-half buckling) (c) Type HC (Half buckling)

Fig. 8 Schematic view of failure modes of hollow steel tubular columns

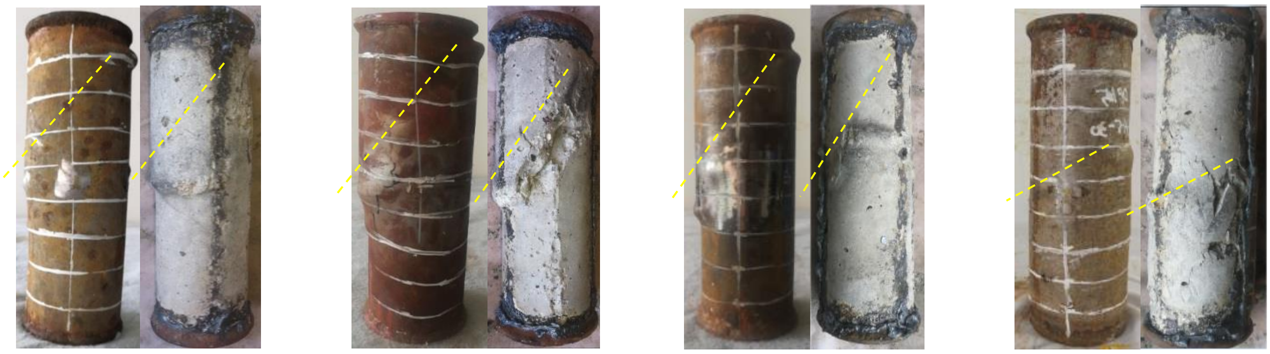

(a) C235-0 (Type CA) (b) C235-5(Type CA) (c) C235-10(Type CA) (d) C235-20(Type CB)

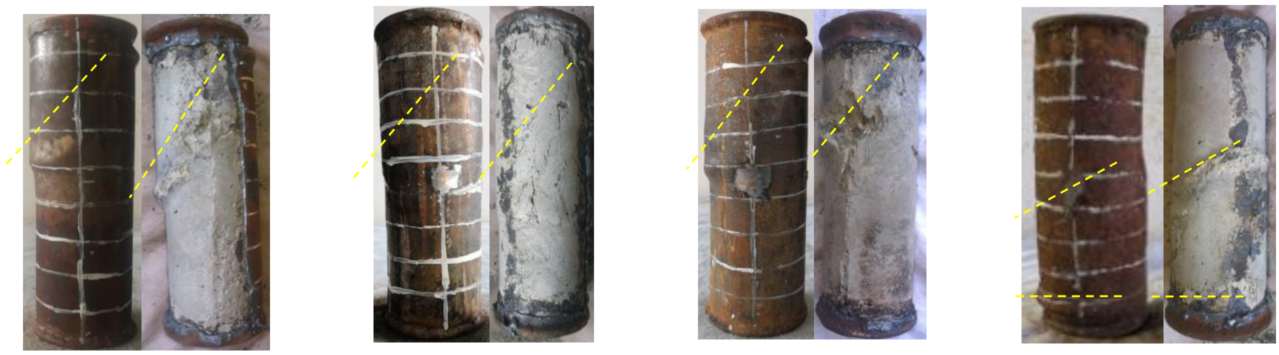

(e) C345-0(Type CA) (f) C345-5(Type CA) (g) C345-10(Type CA) (h) C345-20(Type CC)

Fig. 9 Failure modes of CFST columns

$$\text{Q235}\begin{cases} f_y^r/f_y = 1-1.32D_w \\ f_u^r/f_u = 1-1.63D_w \\ E_s^r/E_s = 1-0.87D_w \\ \varepsilon_u^r/\varepsilon_u = 1-2.97D_w \end{cases}$$
$$\text{Q345}\begin{cases} f_y^r/f_y = 1-1.58D_w \\ f_u^r/f_u = 1-1.11D_w \\ E_s^r/E_s = 1-0.98D_w \\ \varepsilon_u^r/\varepsilon_u = 1-3.46D_w \end{cases} \quad (2)$$

where f_y^r, f_u^r, E_s^r and ε_u^r are yield strength, ultimate strength, Young's modulus of steel and ultimate strain of corroded steel respectively.

It should be mentioned that the key constants in Eq. (2) (especially for predicting the steel strength) in different studies (Zheng *et al*. 2015, Yuan *et al*. 2019) are quite different with each other. The only consensus agreed by these studies is the performance reduction of corroded steel varies linearly with corrosion rate. Some studies (Han *et al*. 2012, 2014) prefer to use a strength reduction factor related to corrosion rate to directly predict the performance reduction of structural member under corrosion, instead of using a reduced strength of corroded steel to assess the performance reduction of structural member. It indicates that the properties reduction of steel is sensitive to the thickness and grade of steel, corrosion method and corrosive solutions.

3.2 Failure modes of specimens

Fig. 7 shows the failure modes of hollow steel tubular column. Besides that, both severe inward and outward local buckling were observed in all the specimens, there are three types of failure modes for hollow steel tubular column according to different local buckling positions, as shown in Fig. 8. It is hard to say the corrosion has significant effects on the failure modes of hollow steel tubular column. It may indicate that by increasing the corrosion rate, the buckling tends to occur in the central area of hollow steel tube, due to the reduction of tube wall thickness and material properties of steel.

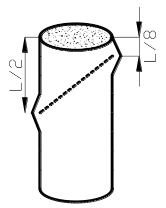

(a) Type CA (50°-55° shear angle)

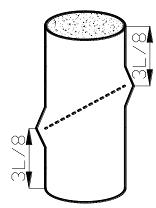

(b) Type CB (30°-35° shear angle)

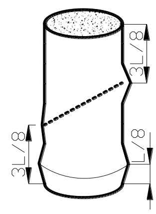

(c) Type CC (30°-35° with bottom buckling)

Fig. 10 Schematic view of failure modes of CFST columns

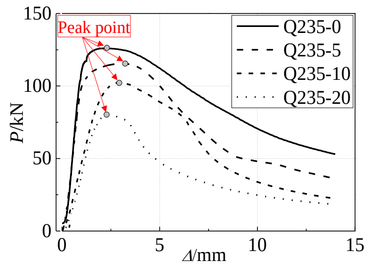

(a) Q235 steel

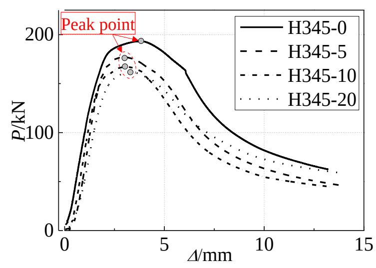

(b) Q345 steel

Fig. 11 Load-displacement curves of hollow steel tubular columns

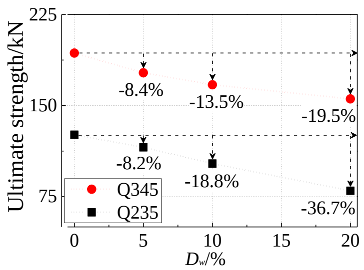

(a) Ultimate strength

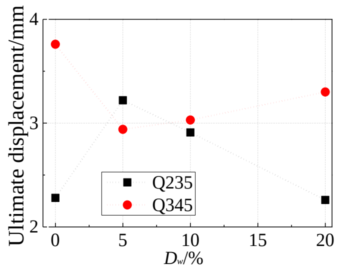

(b) Ultimate displacement

Fig. 12 Ultimate performance comparison of hollow steel tubular columns

Fig. 9 shows the failure modes of CFST column. It can be seen that only outward buckling was observed at the outer steel tubes, due to the support provided by core concrete. After the test, outer steel tubes were removed to observe the failure modes of core concrete. A diagonal shear crack and many micro cracks were observed on the concrete surface. It can be found that the core concrete cracked in the areas where the outer steel tube buckled outward. It may indicate that the shear crack of core concrete results in the outward buckling of the outer steel tube. Fig. 10 shows the schematic view of failure modes of CFST column. It can be seen that all the specimens fail associating with shear. By increasing the corrosion rate, the shear cracking angle of CFST column varies from (50-55) degree to (30-35) degree.

It should be mentioned that even though the failure modes of hollow steel and CFST columns are summarized, it is hard to link the failure modes to corrosion rate directly, since many uncertain factors would affect the failure modes of specimens and the number of tested specimens is not large enough. More studies are worthy to be conducted on the relation between failure mode and corrosion rate.

3.3 Load-displacement curves of specimens

3.3.1 Hollow steel tubular column

Fig. 11 shows the representative curves of steel tubular columns under different corrosion rates. Decreasing of ultimate strength is observed in both the specimens with Q235 steel and Q345 steel, with the increase of corrosion rate. The decrease degree of ultimate strength is larger for specimens with Q235 steel than those with Q345 steel. Even with different failure modes as shown in Figs. 7-8, the trend of curves shows little difference, especially for the specimens with Q345 steel. All the curves are smooth under axial loading.

Fig. 12 shows the relationship of ultimate strength and displacement with corrosion rate. Ultimate displacement is defined as the displacement corresponding to the ultimate strength of specimens in the curves. It can be seen that the ultimate strength of hollow steel tubular column decreases linearly with the increase of corrosion rate. Larger strength reduction is observed in the specimens with Q235 steel. The strength deterioration of the specimens with Q235 steel

(a) Q235 steel (b) Q345 steel

Fig. 13 Load-displacement curves of CFST columns

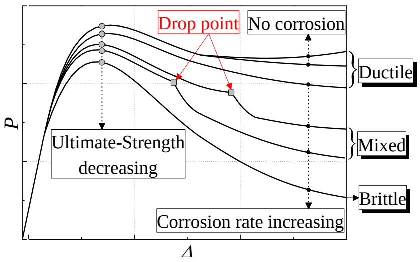

Fig. 14 Relationship of CFST column’s failure mode with corrosion rate

under 20% corrosion rate is 36.7%, which is almost twice larger than that of the specimens with Q345 steel under the same corrosion rate. It may indicate that the hollow steel tubular column with lower steel strength would be more sensitive to corrosion rate, since local buckling would be much easier to occur under unevenly pitting corrosion. Irregular influence of corrosion rate on the ultimate displacement of the specimens is observed. It may indicate that the ultimate displacement of hollow steel tubular column is hardly affected by corrosion rate.

3.3.2 CFST column

Fig. 13 shows the representative curves of CFST columns under different corrosion rates. Similar to the hollow steel specimens, the ultimate strength of both the specimens with Q235 steel and Q345 steel deceases with the increase of corrosion rate. In addition, the curves show quite different trends under different corrosion rate.

As summarized in Fig. 14, the CFST stub column with proper confinement factor shows a ductile failure. The strength of CFST stub column would stay a relatively lower value after the peak point, sometimes may even slightly increase at large deformation, due to the confinement effect of outer steel tube (Zhong 2003). Increasing corrosion rate would change the ductile failure of CFST stub column to brittle failure due to the weakening of confinement effect. A mixed failure curve is also presented which contains both ductile failure and brittle failure. A drop point is observed in these curves of mixed failure curve. After drop point, the failure mode of specimen would alter from ductile failure to brittle failure. The corresponding axial deformation of drop point would be reduced by increasing corrosion rate, as shown in Fig. 13(a). Under 20% corrosion rate, brittle failure mode is observed in the CFST columns using Q235 steel and Q345 steel.

Fig. 15 shows the relationship of ultimate strength and displacement of CFST specimens with corrosion rate. A decrease of ultimate strength is observed with the increase of corrosion rate. Strength reductions of CFST specimens are much smaller than those of the hollow steel tube counterparts. It is due to the fact that inner concrete provides support for hollow steel tube when local buckling happens in the steel tube under pitting corrosion. Also, the strength of steel tube is only a part of the strength of CFST column. Core concrete is not significantly affected by corrosion in steel tube, except for the confinement effect of steel tube. The strength deteriorations of the CFST specimens with Q235 steel under different corrosion rate are all smaller than those of the CFST specimens with Q345 steel. The reason is that Q345 steel tube contributes more to the axial strength of CFST stub column than Q235 steel tube. Therefore, the CFST stub columns using Q345 steel would be more remarkably affected by corrosion than those

(a) Ultimate strength (b) Ultimate displacement

Fig. 15 Ultimate performance comparison of CFST columns

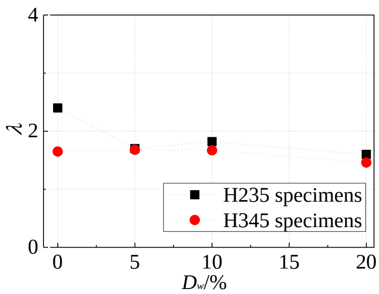

(a) Hollow steel tubular column

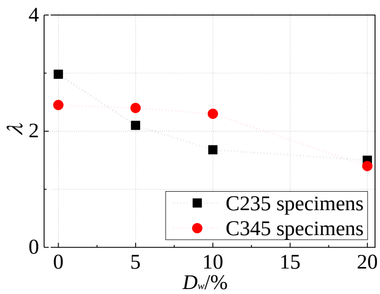

(b) CFST column

Fig. 16 Relationship between ductility index-corrosion rate

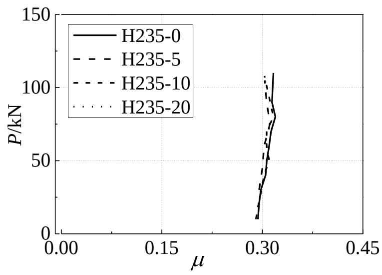

(a) H235 specimens

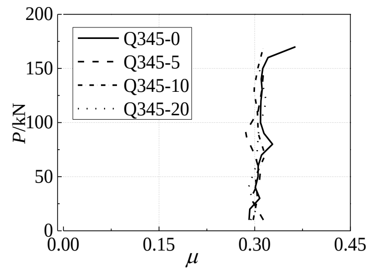

(b) H345 specimens

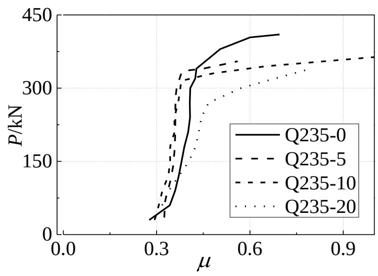

(c) C235 specimen

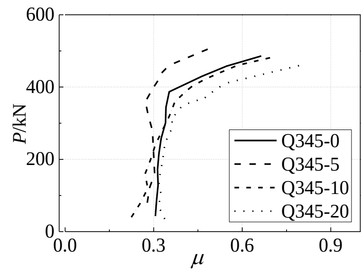

(d) C345 specimen

Fig. 17 Lateral deformation factor of specimens

using Q235 steel.

Irregular influence of corrosion rate on the ultimate displacement of specimens is also observed for CFST column, just like hollow steel tubular column. It implies that corrosion rate also has little influence on the ultimate displacement of CFST column. In fact, the differences among the ultimate displacements of the CFST column specimens under different corrosion rate are rather small.

3.4 Ductility of specimens

To quantify the influence of corrosion rate on the ductility of specimens, a ductility index λ is defined as described in Eq. (3)

$$\lambda = \Delta_{0.85}/\Delta_u \tag{3}$$

where $\Delta_{0.85}$ is the axial displacement of specimen when the applied load falls to 85% of the ultimate load after damage; Δ_u is the axial displacement of specimen when the ultimate strength is reached.

Fig. 16 shows the relationship between ductility index and corrosion rate of hollow steel tubular column and CFST column respectively. The ductility index of hollow steel tubular column is hardly changed by corrosion rate, since the failure mode shown in Fig. 11 is also not affected by corrosion rate. In contrary, the ductility index of CFST column shown in Fig. 16(b) decreases with the increase of corrosion rate, which is also in agreement with the failure mode shown in Figs. 13-14. For instance, the C345 specimens under 0, 5% and 10% corrosion rate exhibit similar failure modes and similar trend P-Δ curves. In that case, the ductility indexes of the C345 specimens under 0, 5% and 10% corrosion rate only decrease slightly. This result could be explained by the fact that the ductility of CFST stub column will decrease with the decrease of confinement effect which is one of the direct effect of corrosion (Han *et al*. 2014).

3.5 Lateral deformation factor of steel tube

Lateral deformation factor μ is defined as the ratio of transverse strain and longitudinal strain of steel tube. The lateral deformation factors of the specimens are illustrated in Fig. 17. It can be seen that the lateral deformation factors of hollow steel tubular column specimens stay around 0.3 in the loading process which equals to the Poisson ratio of steel, due to the absence of in-filled concrete. In contrary, the lateral deformation factors of CFST column specimens remain around 0.3 before the axial load reached 80% of the ultimate strength. After that, lateral deformation factor increases remarkably due to the confinement effect and the axial yield of specimen. It can be seen that the lateral deformation factors of specimens tend to be larger with the increase of corrosion rate. It indicates that the lateral deformation of CFST column becomes larger under corrosion, due to the reduction of the confinement from outer tube to core concrete.

3.6 Confinement effect of CFST column

The nominal strength N_0 and confinement factor ξ of CFST column are respectively defined as

$$N_0 = f_y A_s + f_c A_c \tag{4}$$

$$\xi = f_y A_s / f_c A_c \tag{5}$$

where f_y and f_c are the strength of steel and concrete respectively; A_s and A_c are the area of steel tube and core concrete respectively.

To assess the confinement effect, the ratio of average test value and nominal value $\overline{N}_u / N_0$ is used, as listed in Table 5 and Fig. 18. It can be seen that due to the thickness reduction of steel tube wall under corrosion, the confinement factor ξ decreases with the increase of corrosion rate. In contrary, the ratio of test value and nominal value shows an opposite trend. It indicates that confinement effect would contribute to resist the strength reduction due to corrosion.

4. Discussions

4.1 Hollow steel tubular column

Predicting methods for the axial strength of hollow steel tubular stub column have been covered by various standards, such as Eq. (6) in GB50017 (2017), Eq. (7) in AIJ (2005), Eq. (8) in Eurocode 3 (2007) and Eq. (9) in AISC360-10 (2010). It should be mentioned that corroded steel strength f_y^r described by Eq. (2) is used to replace steel strength f_y in the original methods as follows

$$N_{\mathrm{CN}}^H = \varphi_{\mathrm{CN}} f_y^r A_s \tag{6}$$

$$N_{\mathrm{JP}}^H = \frac{1-0.4\left[\lambda/\sqrt{\pi^2 E_s/(0.6 f_y^r)}\right]^2}{3/2+2/3\left[\lambda/\sqrt{\pi^2 E_s/(0.6 f_y^r)}\right]^2} f_y^r A_s \tag{7}$$

$$N_{\mathrm{EU}}^H = \varphi_{\mathrm{EU}} f_y^r A_s \tag{8}$$

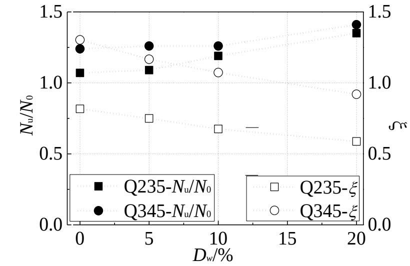

Fig. 18 Confinement effect analysis

Table 5 Analysis of confinement effect

Specimen No.	Test value N_u/kN	Average test value $\overline{N}_u$/kN	Nominal value N_0/kN	$\overline{N}_u / N_0$	ξ	λ
C235-0-1	400.0	402.2	376.8	1.07	1.58	2.98
C235-0-2	404.4					
C235-5-1	383.5	390.7	358.1	1.09	1.45	2.10
C235-5-2	397.9					
C235-10-1	379.5	378.0	318.1	1.19	1.18	1.68
C235-10-2	376.5					
C235-20-1	366.5	360.6	267.8	1.35	0.83	1.50
C235-20-2	354.6					
C345-0-1	538.7	525.0	424.3	1.24	1.92	2.45
C345-0-2	511.2					
C345-5-1	507.6	502.7	396.5	1.26	1.73	2.40
C345-5-2	497.8					
C345-10-1	483.2	479.1	378.1	1.26	1.60	2.30
C345-10-2	475.0					
C345-20-1	463.2	457.8	323.9	1.41	1.23	1.40
C345-20-2	452.5					

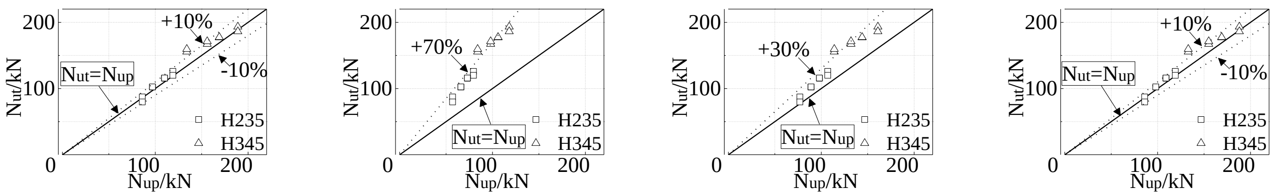

(a) GB50017 (2017) (b) AIJ (2005) (c) Eurocode 3(2007) (d) AISC360-10 (2010)

Note: N_{ut} is tested ultimate strength and N_{up} is predicted ultimate strength

Fig. 19 Comparisons between tested and predicted ultimate strength of hollow steel tubular columns

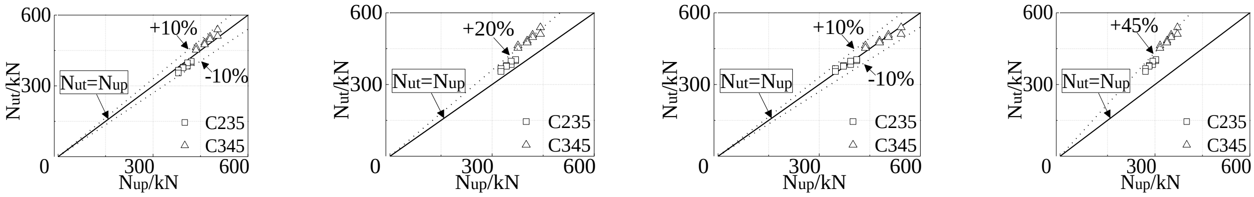

(a) GB50936 (2014) (b) AIJ (2008) (c) Eurocode 4(2004) (d) AISC360-10 (2010)

Note: N_{ut} is tested ultimate strength and N_{up} is predicted ultimate strength

Fig. 20 Comparisons between tested and predicted ultimate strength of CFST columns

$$N_{\mathrm{US}}^{H} = 0.658^{f_y^r/[\pi^2 E_s/(L/r)^2]} f_y^r A_s \tag{9}$$

φ_{CN} and φ_{EU} are the buckling reduction factor in GB50017 (2017) and Eurocode 3 (2007) respectively; λ is slenderness ratio; r is radius of gyration.

Fig. 19 shows the comparison between tested ultimate strength and predicted ultimate strength of hollow steel tubular column. It can be seen that with considering the corrosion, the predicted values by Chinese and US standards match well with the tested values while the predicted values by Japanese standard seem too conservative. Eurocode 3 could provide acceptable predicted values for the specimens using Q235 steel while the predicted values for the specimens using Q345 steel are lower than the tested values by 30%.

4.2 CFST column

In order to evaluate the feasibility of using current design methods to predict the strength of CFST column under simulated marine atmospheric corrosion, Eq. (10) in GB50936 (2014), Eq. (11) in AIJ (2008), Eq. (12) in Eurocode 4 (2004) and Eq. (13) in AISC360-10 (2010) are used to calculate the axial strength of CFST stub column. Corroded steel strength f_y^r described by Eq. (2) is used to replace steel strength f_y in the original methods as follows

$$N_{\mathrm{CN}}^{C} = (A_c + A_s)(1.212 + (\frac{0.176 f_y^r}{213} + 0.974)\ \xi + (\frac{-0.104 f_c}{14.4} + 0.031)\ \xi^2) f_c \tag{10}$$

$$N_{\mathrm{JP}}^{C} = A_c f_c + 1.27 f_y^r A_s \tag{11}$$

$$N_{\mathrm{EU}}^{C} = 0.85 A_c f_c \left[1 + 4.9(\frac{t}{D})\left(\frac{f_y^r}{0.85 f_c}\right)\right] + 0.75 f_y^r A_s \tag{12}$$

$$N_{\mathrm{US}}^{C} = 0.658^{f_y^r/[\pi^2 E_s/(L/r)^2]}\left(f_y^r A_s + 0.85 f_c A_c\right) \tag{13}$$

where ξ is the confinement factor of CFST column.

It can be seen from Fig. 20 that the predicted values by using the corroded steel strength in Chinese and EU standards match well with the tested values. The predicted values from US standard are conservative without considering confinement effect, while those from Japanese standard seem acceptable.

5. Conclusions

This paper aims to study the compressive behavior of circular hollow and concrete-filled steel tubular stub columns in simulated marine atmospheric corrosion. The specimens after salt spray corrosion were tested under axial compressive load. The experimental results are discussed in detail and compared with current design standards. The following conclusions are made:

(1) Simulated marine atmospheric corrosion would cause the degradation of tensile properties of steel. Linear fitting curves could be used to present the relationship between corrosion rate and the mechanical properties of corroded steel.
(2) Both severe inward and outward local buckling were observed at hollow steel tubular column while only outward buckling was observed at the outer

steel tube of CFST, due to the support provided by core concrete. Simulated marine atmospheric corrosion has some effects on the failure mode of CFST column, rather than that of hollow steel tubular column.

(3) The ultimate strength of hollow steel tubular column decreases linearly with the increase of corrosion rate while the ultimate displacement of hollow steel tubular column is hardly affected by corrosion rate. The hollow steel tubular column with lower steel strength would be more sensitive to corrosion rate.
(4) Increasing corrosion rate would change the failure of CFST stub column from ductile failure to brittle failure. Strength reductions of the CFST specimens are much smaller than those of the counterparts while corrosion rate has little influence on the ultimate displacement of CFST column.
(5) The ductility indexes of hollow steel tubular column are hardly changed by corrosion rate, while the ductility indexes of CFST column decrease with the increase of corrosion rate based on the corresponding failure modes. The confinement factor ξ of CFST column decreases with the increase of corrosion rate while the ratio of test value and nominal value shows an opposite trend.
(6) With considering marine atmospheric corrosion, the predicted strength of hollow steel tubular column by using Chinese and US standards match well with the tested values while the predicted values by using Japanese standard seem too conservative.
(7) The predicted strength of CFST column by using the corroded steel strength and Chinese and EU standards match well with the tested values. Without considering confinement effect, the predicted values by using US standard are conservative while those by using Japanese standard seem acceptable.

Acknowledgments

The project is supported by National Natural Science Foundation of China (NO. 51908085), Natural Science Basic Research Program of Shaanxi (No.2019JQ-145), Open fund of Shaanxi Key Laboratory of safety and durability of concrete structures (XJKFJJ201803), The Youth Innovation Team of Shaanxi Universities and Xijing University Special Foundation (XJ17T07) which are gratefully acknowledged.

References

AIJ (2005), Design standard for steel structures-based on allowable stress concept, Architectural Institute of Japan.

AIJ (2008), Recommendations for design and construction of concrete filled steel tubular structures;, Architectural Institute of Japan.

AISC360-10 (2010), Specification for Structural Steel Buildings, American Institute of Steel Construction.

Beaulier, L.V., Legeron, F. and Langlois, S. (2010), “Compression strength of corroded steel angle members”, *J. Constr. Steel Res.*, **66**, 1366-1373. https://doi.org/10.1016/j.jcsr.2010.05.006

Chaves, A.I. and Melchers, E.R. (2011), “Pitting corrosion in pipeline steel weld zones”, *Corrosion Sci.*, **53**, 4026-4032. https://doi.org/10.1016/j.corsci.2011.08.005

Chen, M.C., Zhang, F.M., Huang, H. and Wang, C. (2018), “Study on seismic performance of concrete filled square steel tubes subjected to simulated acid rain attack”, *J. China Railway Soc.*, **40**(6), 106-114. https://doi.org/10.3969/j.issn.1001-8360.2018.06.014

Eurocode 3 (2007), Design of steel structures. Part 1-6: Strength and stability of shell structures, European Committee for Standardization.

Eurocode 4 (2004), Design of composite steel and concrete structures. Part 1-1: general rules and rules for building, European Committee for Standardization.

Gao, S.B., Ikai, T., Ni, J. and Ge, H.B. (2016), “Load-carrying capacity degradation of reinforced concrete piers due to corrosion of wrapped steel plates”, *Steel Compos. Struct., Int. J.*, **20**(1), 91-106. https://doi.org/10.12989/scs.2016.20.1.091

Gao, S.B., Ni, J., Zhang, D.X. and Ge, H.B. (2017), “Strength degradation of reinforced concrete piers wrapped with steel plates under local corrosion”, *Steel Compos. Struct., Int. J.*, **24**(6), 753-765. https://doi.org/10.12989/scs.2017.24.6.753

Han, L.H., Hou, C. and Wang, Q.L. (2012), “Square concrete filled steel tubular members under loading and chloride corrosion: Experiments”, *J. Constr. Steel Res.*, **71**, 11-25. https://doi.org/10.1016/j.jcsr.2011.11.012

Han, L.H., Hou, C.C. and Wang, Q.L. (2014), “Behavior of circular CFST stub columns under sustained load and chloride corrosion”, *J. Constr. Steel Res.*, **103**, 23-36. https://doi.org/10.1016/j.jcsr.2014.07.021

Hou, C.C., Han, L.H., Wang, Q.L. and Hou, C. (2016), “Flexural behavior of circular concrete filled steel tubes (CFST) under sustained load and chloride corrosion”, *Thin-Wall. Struct.*, **107**, 182-196. https://doi.org/10.1016/j.tws.2016.02.020

Hu, J.Y., Liang, H.J. and Lu, Y.Y. (2018), “Behavior of steel-concrete jacketed corrosion-damaged RC columns subjected to eccentric load”, *Steel Compos. Struct., Int. J.*, **29**(6), 689-701. https://doi.org/10.12989/scs.2018.29.6.689

Hua, Y.X., Han, L.H., Wang, Q.L. and Hou, C. (2019), “Behavior of square CFST beam-columns under combined sustained load and corrosion: Experiments”, *Thin-Wall. Struct.*, **136**, 353-366. https://doi.org/10.1016/j.tws.2018.12.037

Jiang, X.L. and Soares, C.G. (2012), “Ultimate capacity of rectangular plates with partial depth pits under uniaxial loads”, *Marine Struct.*, **26**, 27-41. https://doi.org/10.1016/j.marstruc.2011.12.005

Kaita, T., Ruwan, J.M., Appuhamy, S. and Ohga, M. (2012), “An enhanced method of predicting effective thickness of corroded steel plates”, *Steel Compos. Struct., Int. J.*, **12**(5), 379-393. https://doi.org/10.12989/scs.2012.12.5.379

Karagah, H., Shi, C., Dawood, M. and Belarbi, A. (2015), “Experimental investigation of short steel columns with localized corrosion”, *Thin-Wall. Struct.*, **87**, 191-199. https://doi.org/10.1016/j.tws.2014.11.009

Khedmati, M.R., Hadj, Z., Nouriand, M.E. and Roshanali, M.M. (2011), “An effective proposal for strength evaluation of steel plates randomly corroded on both sides under uniaxial compression”, *Steel Compos. Struct., Int. J.*, **11**(3), 183-205. https://doi.org/10.12989/scs.2011.11.3.183

Melchers, R.E. (2003), “Mathematical modeling of the diffusion controlled phase in marine immersion corrosion of mild steel”, *Corrosion Sci.*, **45**, 923-940. https://doi.org/10.1016/S0010-938X(02)00208-1

Qin, S.P. and Cui, W.C. (2003), “Effect of corrosion models on the

time-dependent reliability of steel plated elements", *Marine Eng*., **16**, 15-34.
https://doi.org/10.1016/S0951-8339(02)00028-X
Saad-Eldeen, S., Garbatov, Y. and Soares, C.G. (2013), "Effect of corrosion severity on the ultimate strength of a steel box girder", *Eng. Struct*., **49**, 560-571.
https://doi.org/10.1016/j.engstruct.2012.11.017
GB/T10125 (2012), Corrosion tests in artificial atmospheres-Salt spray tests, Standardization Administration of China.
GB50017 (2017), Standard for design of steel structures, Ministry of Construction of the People's Republic of China.
GB50936 (2014), Technical code for concrete filled steel tubular structures, Ministry of Construction of the People's Republic of China.
Wang, X. and Melchers, E.R. (2017), "Long-term under-deposit pitting corrosion of carbon steel pipes", *Ocean Eng*., **133**, 231-243. https://doi.org/10.1016/j.oceaneng.2017.02.010
Wang, X.M., Wang, P., Sun, Y.C. and Lian, B.J. (2015), "Corrosion Resistance of Q235 Steel in Simulated Marine Atmospheric Environment", *Surface Technol*., **44**(11), 104-111.
Wang, Y.D., Xu, S.H., Wang, H. and Li, A.B. (2017a), "Predicting the residual strength and deformability of corroded steel plate based on the corrosion morphology", *Constr. Build. Mater*., **152**, 777-793.
https://doi.org/10.1016/j.conbuildmat.2017.07.035
Wang, Y.Y., Chen, P., Liu, C.Y. and Zhang, Y. (2017b), "Size effect of circular concrete-filled steel tubular short columns subjected to axial compression", *Thin-Wall. Struct*., **120**, 397-407. https://doi.org/10.1016/j.tws.2017.09.010
Yuan, F., Chen, M.C., Huang, H. and Xie, L (2018), "Circular concrete filled steel tubular columns under cyclic load and acid rain attack: Test simulation", *Thin-Wall. Struct*., **122**, 90-101.
https://doi.org/10.1016/j.tws.2017.10.005
Yuan, F., Chen, M.C. and Huang, H. (2019), "Squre CFST columns under cyclic load and acid rain attack: Test simulation", *Steel Compos. Struct*., *Int. J*., **30**(2), 171-183.
https://doi.org/10.12989/scs.2019.30.2.171
Zhang, S.M., Guo, L.H. and Ye, Z.L. (2005), "Behavior of steel tube and confined high strength concrete fore concrete-filled RHS tubes", *Adv. Struct. Eng*., **8**(2), 101-116.
https://doi.org/10.1260/1369433054037976
Zheng, S.S., Wang, X.F. and Han, Y.Z. (2015), "Experimental research on seismic behavior of multi-aged steel frame columns under acidic atmospheric environment", *China Civil Eng. J*., **48**(8), 47-59.
Zhong, S.T. (2003), The Concrete-Filled Steel Tubular Structures, Tsinghua University Press, Beijing, China.

DL